scientific reports

Check for updates

OPEN

Helium cold atmospheric pressure plasma reduces erastin induced inflammation and ferroptosis in human gingival fibroblasts

Jung Sun Park[1,3], Young-Il Jeong[1,3] & Byung-Hoon Kim[1,2]✉

Oral soft tissue damage can lead to hard tissue damage in the oral cavity, such as periodontal lesions, periapical disorders, cysts, and oral tumors. Cold plasma is known to alleviate inflammation and oxidative stress and promote tissue regeneration, yet the effects of helium plasma on human gingival cells remain poorly understood. In this study, we examined whether helium (He) cold atmospheric pressure plasma (CAP) can induce anti-inflammatory and anti-ferroptotic effects in oral soft tissues by ionizing He gas. Erastin treatment followed by He CAP exposure in human gingival fibroblast-1 (HGF-1) cells reduced the mRNA expression of inducible nitric oxide synthase (iNOS), cyclooxygenase-2 (COX-2), interleukin-1β (IL-1β), tumor necrosis factor-α (TNFα), and interleukin-6 (IL-6), which are linked to inflammatory responses. Additionally, He CAP exposure decreased nuclear receptor coactivator 4 (NCOA4) expression and increased glutathione peroxidase 4 (GPX4) expression. Furthermore, mitochondrial membrane potential was restored by increased voltage-dependent anion channel 1 (VDAC1) expression, and reactive oxygen species (ROS) levels in mitochondria and cytoplasm were reduced. These results suggest that He CAP exposure may be associated with modulation of mitochondrial ROS production and reduction of inflammation and ferroptosis, but whether mitochondrial repair contributes to these effects requires further investigation.

Keywords Ferroptosis, GPX4, Iron, VDAC1, He cold atmosphere pressure plasma, INOS

Abbreviations

CAP	cold atmospheric pressure plasmas
CM-H2DCFDA	5,6-chloromethyl-2′,7′-dichlorodihydrofluorescein diacetate
FHC	ferritin heavy chain
FLC	ferritin light chain
GPX4	glutathione peroxidase 4
He	Helium
HGF-1	human gingival fibroblasts-1
IL-1β	interleukin-1β
IL-6	interleukin-6
iNOS	inducible nitric oxide synthase
SLM	Standard Liter per Minute
ΔΨm	mitochondrial membrane potential
NCOA4	Nuclear Receptor Coactivator 4
TNF-α	tumor necrosis factor-α
VDAC-1	voltage-dependent anion-selective channel 1

Periodontitis is an inflammatory disease of the periodontium and includes gingivitis, periodontitis, pericoronitis, and gingival abscess[1,2], which cause bleeding, swelling, pain, fever, and degradation of the periodontal tissue around the teeth. Further disease progression leads to loss of tooth support and tooth[3,4]. Gingival fibroblasts are involved in the movement, division, and growth of cells within periodontal tissue, and play a role in regulating

[1]Convergence Research Center for Treatment of Oral Soft Tissue Disease (MRC), 7 Chosundaegil, Gwangju 61452, Republic of Korea. [2]Department of Dental Materials, School of Dentistry, Chosun University, 7 Chosundaegil, Gwangju 61452, Republic of Korea. [3]Jung Sun Park and Young-Il Jeong contributed equally. ✉email: kim5055@chosun.ac.kr

the immune status of periodontal tissue through interactions with immune cells[5–8]. Therefore, inflammation treatment of gingival fibroblast leads to the interaction of tissue and inflammatory mediators, promoting damaged tissue regeneration, secreted cytokine regulation, and periodontal tissue recovery[9,10]. However, persistent inflammation and oxidative stress can disrupt normal cellular processes, creating conditions that lead to ferroptosis[11–13].

Ferroptosis is a cell death mechanism that occurs when the balance of iron metabolism is disrupted, resulting in structural and functional damage to cell membranes[14,15]. Excessive accumulation of ferrous ions triggers the Fenton reaction, reduces the expression of the lipid peroxidation inhibitor glutathione peroxidase 4 (GPX4), and generates reactive oxygen species (ROS). Periodontal disease, oral tumors, smoking, excessive drinking, and irregular oral hygiene increase oxidative stress in the oral cavity and decrease GPX4 levels[16–18].

Helium cold atmospheric pressure plasma (He CAP) is a partially ionized gas generated under atmospheric pressure conditions, utilizing helium as the carrier gas[19,20]. It produces a unique reactive environment containing various reactive oxygen species (ROS), reactive nitrogen species (RNS), and ultraviolet (UV) photons, which can interact with biological tissues and cells[21,22]. As a result, He CAP has attracted considerable attention in biomedical applications due to its ability to induce controlled oxidative stress, modulate cellular functions, and promote therapeutic effects without causing thermal damage to surrounding tissues. Currently, bio-related research is reporting studies that apply the characteristics of low-temperature plasma to enable removal of microorganisms, treatment of skin inflammation, and tissue regeneration[23–25]. Particularly, several studies have focusses on biological applications such as cell and tissue treatment and bacterial sterilization using He CAP[26–28]. While the role of He CAP in the pathogenesis or treatment of various inflammatory diseases is increasingly being focused on, only a few data have been reported in the literature on the potential use of He CAP in the treatment of periodontitis. Since oral soft tissue damage is often associated with persistent inflammation and oxidative stress as a precursor of periodontal diseases, including periodontitis, addressing these factors is important to prevent disease progression. In addition, recent studies have shown that ferroptosis, a regulated form of cell death induced by iron and lipid peroxidation, is associated with inflammatory diseases, including periodontitis[29,30]. Given the pivotal role of gingival fibroblasts in periodontal health and disease, we hypothesized that He CAP, which has promising potential in reducing inflammation and promoting tissue regeneration in other biomedical fields, may contribute to reducing inflammation and ferroptosis in gingival fibroblasts. Therefore, in this study, we aimed to investigate the effects of He CAP on reducing inflammation and ferroptosis in gingival fibroblasts. This suggests that He CAP may represent a promising and alternative direction for the pathogenesis or treatment of periodontitis based on its effects on periodontal tissues.

Results

Inflammatory response and induction of ferroptosis by Erastin treatment in HGF-1 cells.

In this study, erastin, which induces inflammation, was used to simultaneously model oxidative stress and ferroptosis, which are causes of periodontal tissue damage. Erastin is a well-established ferroptosis inducer that depletes glutathione and generates excessive ROS, leading to lipid peroxidation and cell damage. We investigated the expression of inflammatory cytokines and genes associated with ferroptosis in HGF-1 after erastin treatment. After treatment with 10 μM erastin for 6 h, the mRNA expression of iNOS, COX-2, IL-1β, TNFα, and IL-6 was significantly increased compared to the control group (Fig. 1A). To observe iNOS and COX-2 protein expression, the cells were treated with erastin at concentrations of 0, 5, 10, and 20 μM for 6 h. Protein expression increased starting with 5 μM erastin treatment (Fig. 1B). Fluorescence-activated cell sorting (FACS) analysis of intracellular cytokines IL-1β, TNFα, and IL-6 observed a right shift compared to the IgG control group after treatment with 10 μM Erastin (Fig. 1C). Next, we stimulated cells with erastin and observed the mRNA and protein expression of GPX4, whose expression decreased when ferroptosis progressed. GPX4 mRNA expression decreased in a time-dependent manner, showing a decrease of more than 50% when treated for 6 h (Fig. 1D). GPX4 protein expression decreased in a dose-dependent manner with erastin treatment, and the expression levels of ferritin heavy chain (FHC) and ferritin light chain (FLC), which are involved in intracellular iron metabolism and oxidative stress, also decreased (Fig. 1E). The mRNA and protein expression of nuclear receptor coactivator 4 (NCOA4), a protein that promotes ferroptosis, increased in a concentration-dependent manner during 6 h of erastin treatment (Fig. 1F-G). These results show that treatment of human gingival cells with erastin increases the expression of pro-inflammatory cytokines, decreases GPX4 and increases NCOA4 expression related to ferroptosis.

Expression of inflammatory cytokines and GPX4 by he CAP exposure in HGF-1 cells

Next, we studied the conditions of He CAP exposure time and helium gas flow on the expression of inflammatory cytokines and GPX4 in HGF-1 cells. For He CAP exposure, a plasma generating nozzle was manufactured with 8 lines, and cell survival rate was observed in a time-dependent manner under 4 L gas flow conditions of He CAP. An increase in lactate dehydrogenase (LDH), indicative of decreased cell viability, was seen starting from 30 s exposure to He CAP (Fig. 2A). Based on Helium CAP processing conditions, temperature changes, electrical properties, oscilloscope and optical emission spectrum (OES) analysis were measured (Fig. 2B-D). Through this analysis, the expression of iNOS, IL-1β, TNFα, and IL-6 mRNA in response to gas flow and exposure time of plasma (He CAP) was determined. Exposure to 0, 15, 30, and 60 s at 4 slm (standard liters per minute) of He CAP showed decreased iNOS, IL-1β, TNFα, and IL-6 mRNA expression (Fig. 3A). Upon 15 s exposure of He CAP at 0, 1, 3, and 4 slm gas flows, iNOS, IL-1β, TNFα, and IL-6 mRNA expression was most reduced at 4 slm (Fig. 3B). The mRNA expression of GPX4 showed a significant increase at 4 slm gas flow upon 15 s exposure of He CAP (Fig. 3C). Immunofluorescence staining of GPX4 occurred in a time-dependent manner under He CAP 4 slm gas flow. There was a significant increase in GPX4 fluorescence at 15 s of He CAP exposure, and a

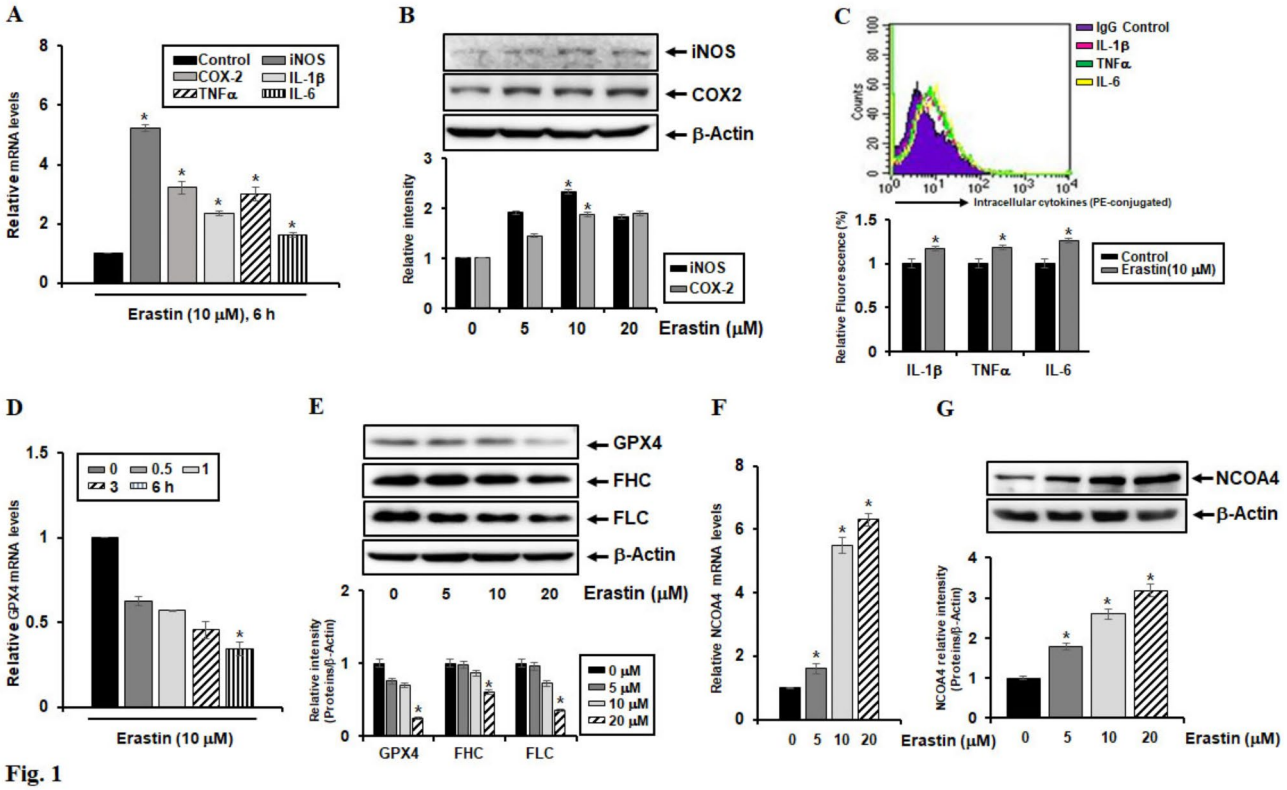

Fig. 1

Fig. 1. Response of inflammatory cytokines to erastin treatment in human gingival fibroblast-1 (HGF-1) cells. (**A**) mRNA expression of inflammatory cytokines iNOS, COX-2, IL-1β, TNFα, and IL-6 after 6 h treatment with 10 μM erastin in HGF-1 cells. The value of the control group was set to 1. (**B**) Protein expression of iNOS and COX-2 was observed using western blotting after treatment with erastin in a concentration-dependent manner. The lower bar graph shows the relative protein levels. (**C**) Intracellular expression of inflammatory cytokines IL-1β, TNFα, and IL-6 after treatment with 10 μM erastin was observed using FACS analysis. The lower graph shows the relative fluorescence values of IL-1β, TNFα, and IL-6 (control was set to 1). (**D**) GPX4 mRNA expression was analyzed after time-dependent treatment with 10 μM erastin. The value of the control group was set to 1. (**E**) Protein expression of glutathione peroxidase 4 (GPX4), ferritin heavy chain (FHC), and ferritin light chain (FLC) was observed using immunoblotting after erastin treatment in a concentration-dependent manner for 6 h. GPX4, FHC, and FLC expression decreased in a concentration-dependent manner. The lower bar graph shows the relative protein levels. (**F**) Nuclear receptor coactivator 4 (NCOA4) mRNA expression was analyzed using qRT-PCR after treatment with erastin at concentrations of 0, 5, 10, and 20 μM for 6 h. NCOA4 expression significantly increased under erastin 10 μM, 6 h conditions. (**G**) NCOA4 protein expression was observed to increase during 6 h of erastin treatment in a concentration-dependent manner. The lower bar graph shows the relative protein levels. All values are presented as the mean ± SD. Statistical significance was measured using Mann–Whitney test. *, $P < 0.05$, compared with the control.

significant decrease in GPX4 expression after 120 s (Fig. 3D). These results suggest that He CAP exposure time and gas flow could modulate the levels of inflammatory cytokines and GPX4 in oral cells.

He CAP effect on inflammatory cytokines and ferroptosis in erastin-treated HGF-1 cells

Based on these results, we investigated whether He CAP regulates inflammatory cytokines and ferroptosis in erastin-induced HGF-1 cells. The increase in erastin-induced iNOS and COX-2 mRNA and protein expression was reduced after exposure to 4 slm He CAP for 15 s (Fig. 4A-B). Using FACS analysis, we show that erastin-induced intracellular expression of iNOS and COX-2 was reduced after He CAP exposure (Fig. 4C). The increase in inflammatory cytokines IL-1β, TNFα and IL-6 mRNA expression by Erastin treatment was reduced after 15 Sec 4 slm of He CAP exposure (Fig. 4D). The decrease in GPX4 protein expression caused by erastin treatment was recovered after He CAP treatment. Conversely, the increase in NCOA4 protein expression caused by erastin treatment was reduced after He CAP treatment (Fig. 4E). Next, reduced glutathione (GSH) and oxidized glutathione (GSSG) levels were measured as indicators of oxidative stress, which can lead to ferroptosis. Additionally, the potential generation of free radicals and lipid peroxides was examined. The GSH/GSH disulfide (GSH/GSSG) ratio was restored upon He CAP exposure (Fig. 4F). Lipid peroxidation was detected by measuring malondialdehyde (MDA), one of the end products of polyunsaturated fatty acid peroxidation in cells. Lipid peroxidation levels were increased by erastin treatment and lowered by He CAP exposure (Fig. 4G). These results suggest that He CAP is potentially involved in modulating the ferroptosis response of oral gingival cells.

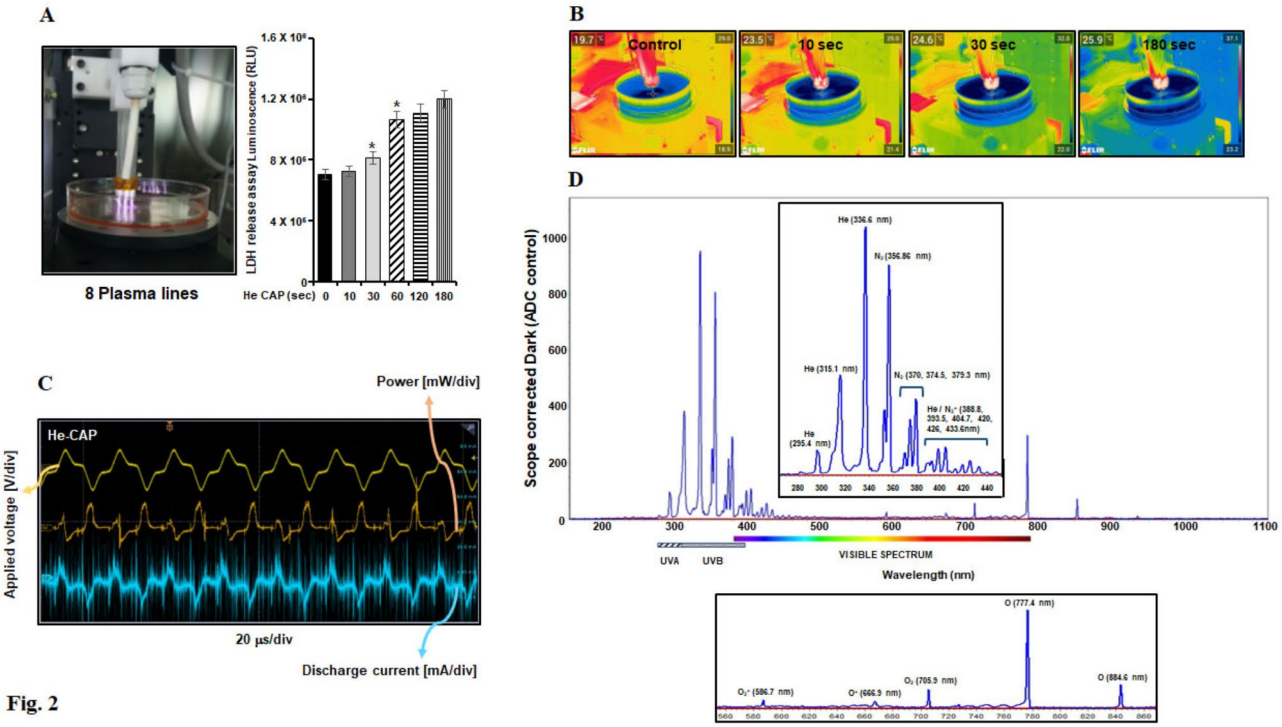

Fig. 2

Fig. 2. Floating Electrode Dielectric Barrier Discharge (FEDBD) plasma device. (**A**) Plasma emitting components are tied together to create eight plasma lines. HGF-1 cells were exposed to He CAP 4 slm in a time-dependent manner and the release of lactate dehydrogenase (LDH) was analyzed using LDH-Glo. He CAP showed an increase in luminescence signal with exposure time. (**B**) Shows the image sensor electronic temperature measurement according to He CAP treatment time. He CAP was measured for 0, 10, 30, and 180 s, and temperature was found to increase with time. (**C**) Electrical characteristics of the current-voltage waveform of helium plasma were shown using an oscilloscope at 6 kV/40 kHz. (**D**) Optical emission spectra (OES) for helium and oxygen showing emission lines of He, O2+, O+, O2, and O in the range of 280 to 860 nm. All values are presented as the mean ± SD. Statistical significance was measured using Mann-Whitney test. *, $P < 0.05$, compared with the control.

He CAP effect on mitochondrial response and voltage-dependent anion channel 1 (VDAC1) expression by erastin treatment in HGF-1 cells

Next, we investigated the mitochondrial response to short-term exposure of He CAP with respect to ROS affecting ferroptosis. The mitochondrial membrane potential was observed under He CAP exposure conditions of 15 s and 4 slm. Green fluorescence, indicative of mitochondrial damage, was increased by erastin treatment and decreased by He CAP exposure (Fig. 5A). We observed VDAC1, a multifunctional protein that plays a pivotal role in maintaining mitochondrial function. VDAC1, located in the mitochondrial outer membrane, shows increased immunofluorescence staining (red) after He CAP exposure (Fig. 5B). We observed VDAC1 protein expression after exposure to He CAP in a time-dependent manner. Short-term exposure to He CAP increased VDAC1 protein expression (Fig. 5C). Next, we studied mitochondrial and cytosolic ROS production after He CAP exposure. Chloromethyl derivative of H2DCFDA (CM-H2DCFDA) and mitochondria-specific superoxide indicator (MitoSOX) fluorescence staining results showed that ROS production in the cytoplasm (green) and mitochondria (red) increased after erastin treatment and decreased after He CAP exposure. N-acetylcysteine (NAC) was used as a positive control (Fig. 5D). Next, we observed the mRNA and protein expression of VDAC1 after exposure to He CAP in erastin-induced cells. Expression of VDAC1 was shown to be increased by He CAP exposure (Fig. 6A-B). Mitochondrial calcium concentration varies with changes in membrane potential. Rhod-2 AM fluorescence was used to observe mitochondrial calcium release. Rhod-2 AM fluorescence, which was reduced by erastin treatment, was restored after He CAP exposure (Fig. 6C). A schematic diagram is shown based on the above results (Fig. 6D).

Discussion

This study has demonstrated that erastin-induced expression of inflammatory cytokines and ferroptosis was reduced by He CAP exposure. Erastin treatment increased the expression of the inflammatory cytokines iNOS, COX-2, IL-1β, TNFα, and IL-6 and ferroptosis-related genes NCOA4 but decreased GPX4 expression. The established He CAP exposure conditions were 4 slm for 15 s for recovery of inflammatory cytokine and ferroptosis expression levels. Prolonging He CAP exposure time decreased GPX4 expression, mitochondrial membrane potential, and cell viability. Under He CAP 4 slm 15 s conditions, the expression of inflammatory

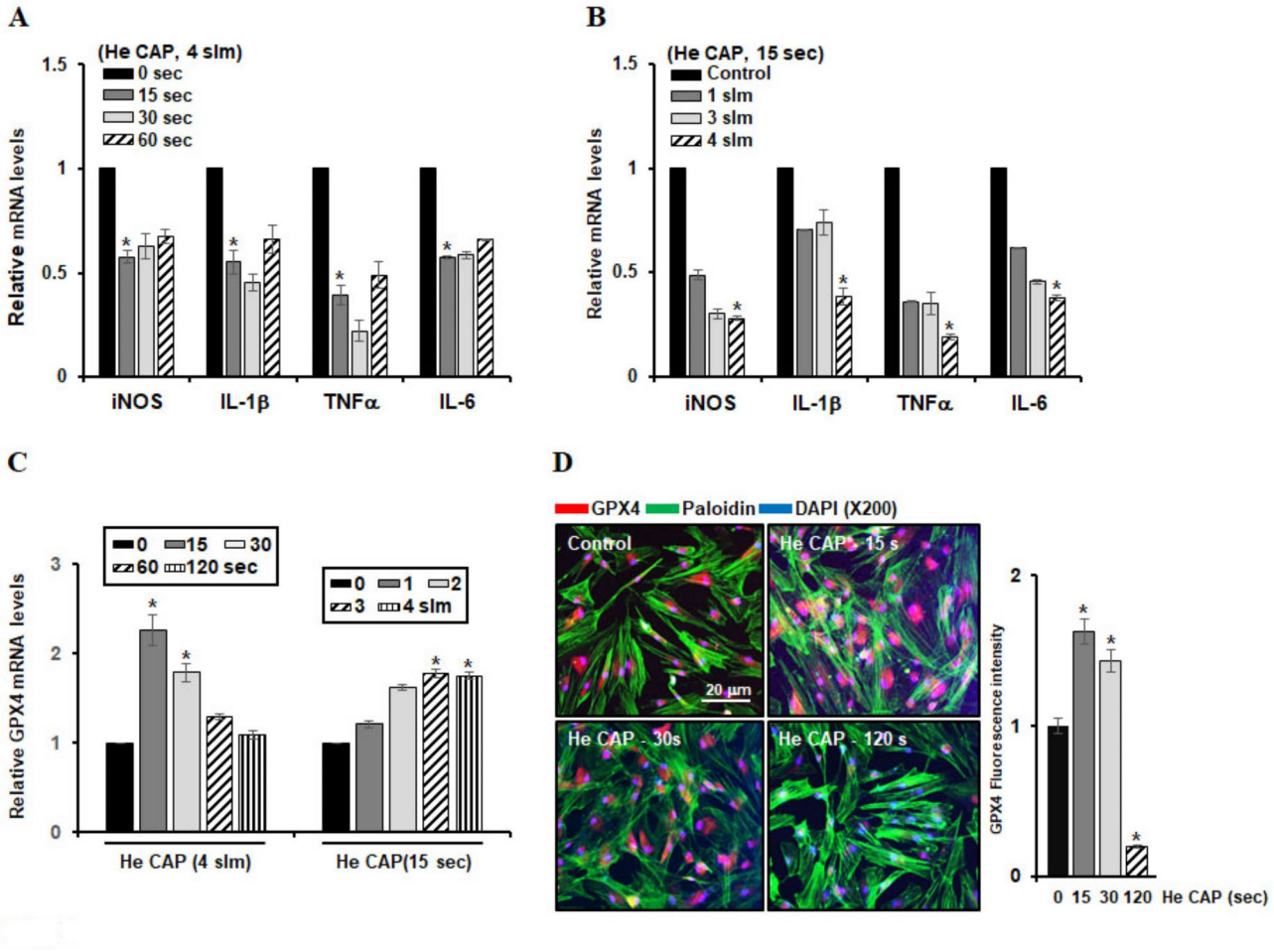

Fig. 3. Expression of inflammatory cytokines and GPX4 in HGF-1 cells after He CAP exposure. (**A**) iNOS, IL-1β, TNFα, and IL-6 mRNA expression was analyzed using qRT-PCR upon exposure to 4 slm He CAP in a time-dependent manner. The value of the control group was set to 1. (**B**) iNOS, IL-1β, TNFα, and IL-6 mRNA expression was analyzed by 15 s exposure to He CAP with 0, 1, 3, and 4 slm helium gas flow. The value of the control group was set to 1. (**C**) GPX4 mRNA expression was analyzed after exposure to He CAP in a time- and gas-flow-dependent manner. The value of the control group was set to 1. (**D**) Immunofluorescence staining of GPX4 was observed after exposure of He CAP to HGF-1 cells. At 15 s of He CAP, fluorescence expression of GPX4 (red) increased. Palloidin, which was used for F-actin staining, showed green fluorescence, and 4',6-Diamidino-2-phenylindole dihydroclide (DAPI), which was used for nuclear staining, showed blue fluorescence. Original magnification, 200 X. Scale bar, 20 μm. The right bar graph shows fluorescence intensity (control set to 1). All values are presented as the mean ± SD. Statistical significance was measured using the Mann-Whitney test. *, $P < 0.05$, compared with the control.

cytokines iNOS, COX-2, IL-1β, TNFα, and IL-6 and NCOA4 were decreased. However, GPX4 expression was increased. Additionally, He CAP exposure increased mitochondrial VDAC1 expression levels and restored mitochondrial membrane potential. These results suggest a potential association of He CAP with mitochondrial recovery and reduced inflammation and ferroptosis in oral cells, but further studies are needed to elucidate the exact mechanism by which mitochondrial recovery is involved in regulating inflammation and ferroptosis.

Periodontal inflammation occurs during incidence of systemic diseases such as diabetes, cardiovascular disease, rheumatoid arthritis, osteoporosis, autoimmune disease, and obesity and during hormonal changes; however, it also occurs as a result of immune regulation disorders, apoptosis, and collagen decomposition caused by various environmental factors[31–33]. These diseases are associated with inflammatory responses, and the imbalance between ROS and iron levels acts as an important factor regulating the inflammatory response, further aggravating the progression of inflammatory diseases and causing cell death such as ferroptosis[34,35]. Treatment methods for periodontal inflammation include appropriate use of antibiotics, periodontal surgery, and removal of dead tissue. However, if there is a treatment that attenuates cell death caused by ferroptosis in periodontal inflammation, it will be helpful in treating periodontal disease.

Ferroptosis is a non-apoptotic iron-dependent form of cell death, in which the reduced form of iron ions (Fe(II)) interacts with oxygen within the cell to generate free radicals. This enhances Fenton reaction and lipid peroxidation. Erastin is a ferroptosis inducer. The inhibition of cysteine-glutamate transporter (system XC-)

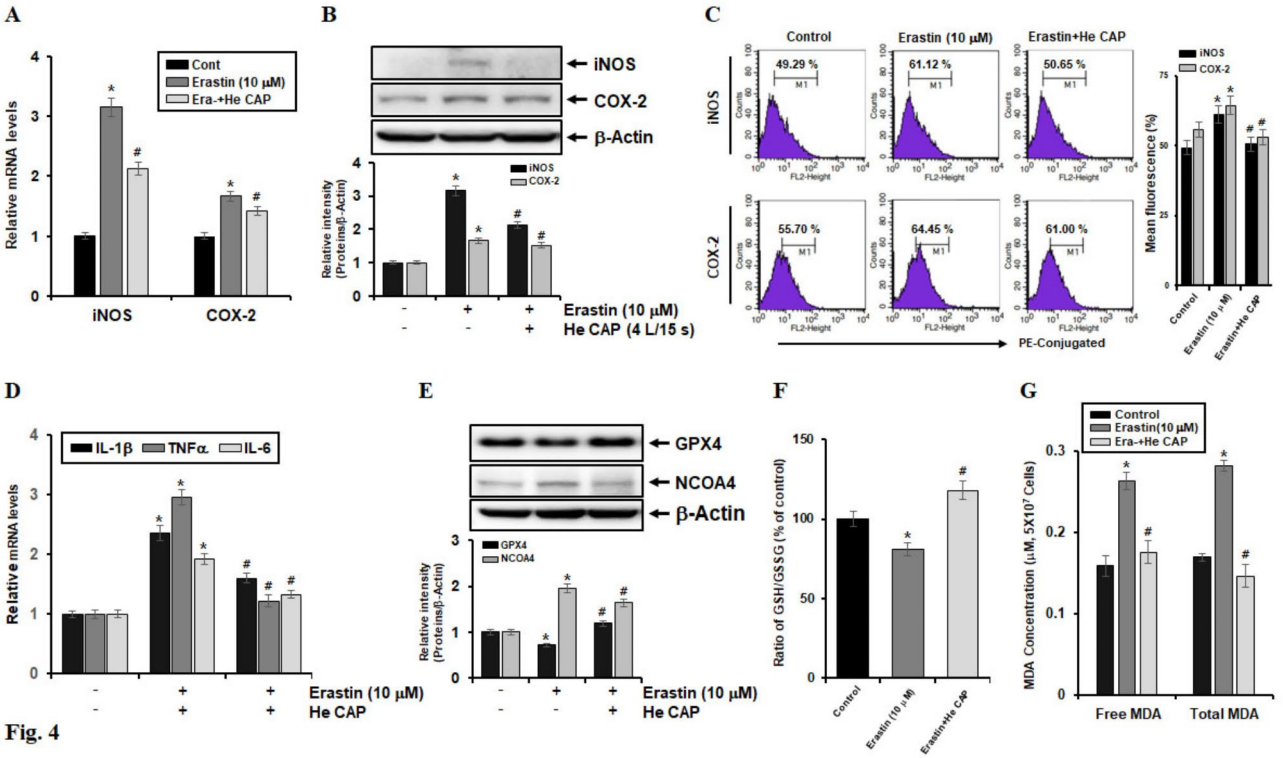

Fig. 4

Fig. 4. Effect of He CAP exposure on the expression of inflammatory cytokines and ferroptosis induced by erastin in HGF-1 cells. (**A**) iNOS and COX-2 mRNA expression in 10 μM erastin treated HGF-1 was analyzed after 15 s exposure to He CAP 4 slm. The value of the control group was set to 1. (**B**) iNOS and COX-2 protein expression in 10 μM erastin treated HGF-1 was analyzed after 15 s exposure to He CAP 4 slm. The bottom bar graph shows the relative protein levels. (**C**) Cells pretreated with 10 μM of erastin were exposed with He CAP, and iNOS and COX-2 expression was observed using FACS analysis. The graph on the right shows the mean value of iNOS and COX-2 fluorescence. (**D**) Cells pretreated with 10 μM erastin were exposed to He CAP and analyzed for mRNA expression of the inflammatory cytokines IL-1β, TNFα, and IL-6. The value of the control group was set to 1. (**E**) Cells pretreated with 10 μM erastin were exposed to He CAP for 4 slm 15 s, and protein expression of GPX4 and NCOA4 was observed using Western blot. The bottom bar graph shows the relative protein levels. (**F**) Cells pretreated with 10 μM erastin were exposed to He CAP at 4 slm for 15 s and reduced/oxidized forms of glutathione were observed. He CAP exposure increased the erastin treatment-reduced glutathione level. GSH/GSSG ratio is shown compared to control. (**G**) Malondialdehyde (MDA) analysis was performed to observe the degree of lipid peroxidation induced by erastin treatment in HGF-1 cells. He CAP exposure of 4 slm for 15 s reduced free and total MDA levels. Relative MDA levels compared to controls are shown. All values are presented as the mean ± SD. Statistical significance was measured using the Mann-Whitney test. *, $P < 0.05$, compared with the control. #, $P < 0.05$, Comparison with cells treated with 10 μM erastin.

by erastin decreases intracellular cysteine concentration, which inhibits glutathione production and increases cellular oxidative stress[36,37]. In this study, treatment of HGF-1 cells with erastin increased cellular ROS, lipid peroxidation, and decreased GPX4 expression. This is the result of erastin causing ferroptosis in oral cells.

Plasma is used practically in a variety of fields, and an appropriate plasma generation method must be selected depending on the purpose. Currently, active research and plasma application are underway in the modern medical field, especially in dentistry, with respect to the plasma type and its method of generation[23,38]. For example, the properties of cold plasma (generated at atmospheric pressure using high-voltage currents) to activate cells by inducing chemical reactions and modulation electron density have been exploited for microbial sterilization, cell and tissue treatment using He CAP. Additionally, biological applications are being researched[39,40]. The CAP used in this study is produced by applying power to generate a voltage between the electrode and the gas, which positively ionizes the surrounding gas molecules through loss of electrons and simultaneously creates free electrons. The free electrons generated within the plasma collide with the surrounding molecules and turn into chemically active radicals that induce various chemical reactions. The mitochondrial membrane inside the cell contains the electron transport chain, where electron transfer and ion exchange occur simultaneously. The results of this study showed that exposure to He CAP for more than 30 s resulted in a decrease in mitochondrial membrane potential proteins and GPX4 expression (Figs. 3C-D and 5C). However, a short exposure time of approximately 15 s increased mitochondrial VDAC1 expression and restored membrane potential and calcium ion concentration (Figs. 5B-C and 6C). The exact mechanism underlying the interaction

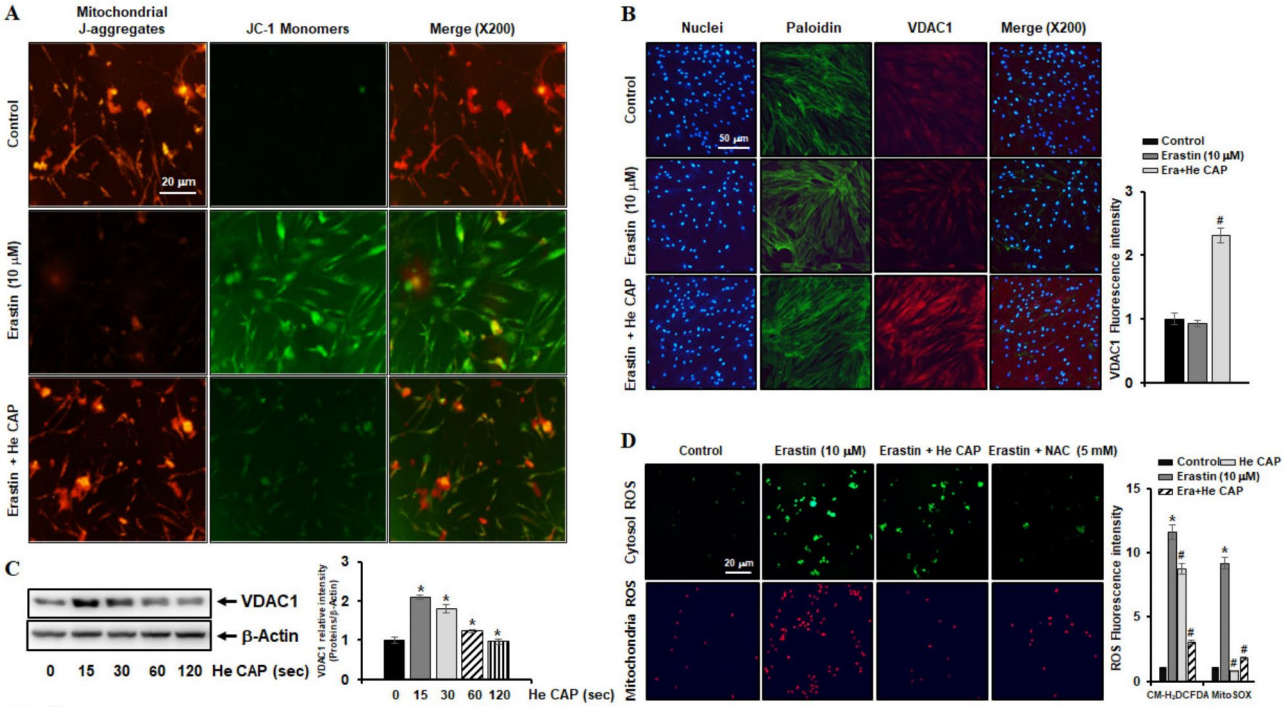

Fig. 5

Fig. 5. Effect of He CAP exposure on voltage-dependent anion-selective channel 1 (VDAC1) expression and mitochondrial membrane potential in HGF-1 cells. (**A**) After exposure of cells pretreated with 10 μM erastin to He CAP, JC-1 fluorescence staining was observed. Recovery of mitochondrial membrane potential was observed upon He CAP exposure. Original magnification, 200 X. Scale bar, 20 μm. (**B**) Cells pretreated with 10 μM erastin were exposed to He CAP and VDAC1 expression (red) was observed through immunofluorescence staining. Immunofluorescence expression of VDAC1 (red) increased in cells exposed to He CAP 4 slm for 15 s. Original magnification, 200 X. Scale bar, 50 μm. The right bar graph shows fluorescence intensity (control set to 1). (**C**) After exposure in He CAP 4 slm in a time-dependent manner, VDAC1 protein expression was observed using Western blotting. VDAC1 expression was found to be significantly increased at 15 s of exposure. The bar graph on the right shows the relative protein levels. (**D**) After treating 10 μM erastin pretreated cells with He CAP and 5 mM NAC, ROS expression was observed in the cytoplasm and mitochondria. After 15 s exposure in He CAP 4 slm, ROS levels were lower in mitochondria than cytoplasm compared to erastin treated cells. Original magnification, 200 X. Scale bar, 20 μm. The right bar graph shows ROS fluorescence intensity. All values are presented as the mean ± SD. Statistical significance was measured using the Mann-Whitney test. *, $P < 0.05$, compared with the control. #, $P < 0.05$, Comparison with cells treated with 10 μM erastin.

between He CAP and free electrons and ions generated and released from the mitochondria remains unknown. However, in erastin-induced HGF-1 cells, ROS levels were attenuated to a greater extent in the mitochondria than in the cytoplasm by He CAP exposure (Fig. 5D). Additionally, it is known that ROS reduction by restoring mitochondrial function reduces cellular lipid peroxidation[41,42]. Treatment with He CAP in erastin-induced HGF-1 cells decreased free and total MDA levels and reduced lipid peroxidation (Fig. 4G). These consequences ultimately weaken the ferroptosis progression. This study demonstrates that He CAP exposure modulates inflammation and ferroptosis-related pathways in periodontal tissues. Although further studies on the precise mechanisms are needed to validate the therapeutic potential of He CAP, it highlights the potential of He CAP as a novel approach to modulate oral inflammation and ferroptosis.

Materials and methods

Antibodies and reagents.

The following antibodies were purchased: GPX4 (ab125066), FHC (ab65080), and FLC (ab69090) from Abcam (Cambridge, UK); Nuclear Receptor Coactivator 4 (NCOA4; 66849), VDAC1 (4661), COX-2 (12282), and iNOS (20609) from Cell Signaling; mouse β-actin antibody (a5316) from Sigma-Aldrich, Inc.; erastin (HY-15763) from MedChemExpress; Cy3 goat anti-rabbit antibody (ab6939) and Alexa Fluor 488 palloidin (A12379) for use as secondary antibodies in immunofluorescence from Abcam and Thermo Fisher Scientific, Inc.

Cell culture

Human gingival fibroblast cells (HGF-1, ATCC CRL-2014, Manassas, VA, USA) were cultured in Dulbecco's Modified Eagles Medium (DMEM) (SH30243.01, HyClone, USA), which was supplemented with 10%

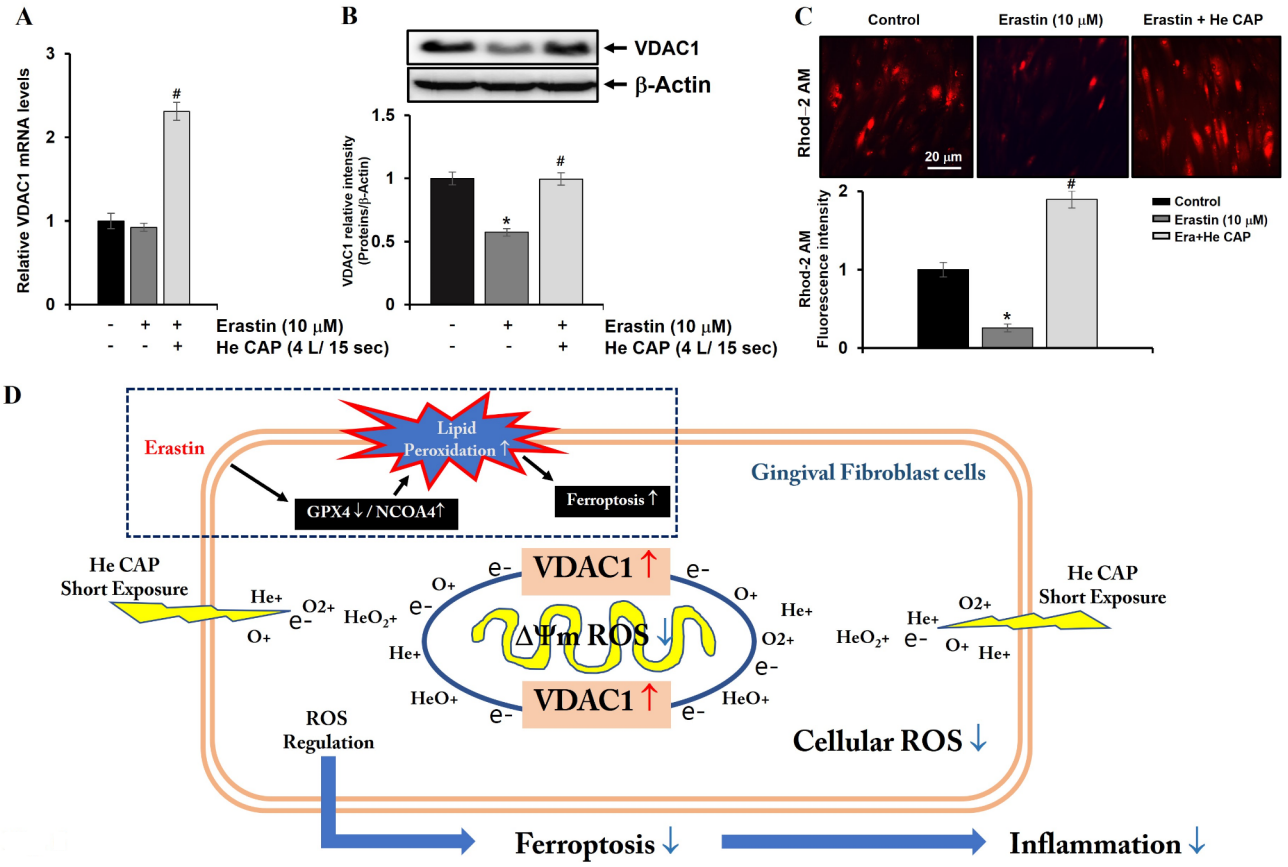

Fig. 6. VDAC1 and calcium concentration response to He CAP exposure in HGF-1 cells. (**A**) VDAC1 mRNA expression was significantly increased after 15 s exposure to He CAP 4 slm. The value of the control group was set to 1. (**B**) Cells pretreated with 10 μM erastin were exposed to He CAP, and VDAC1 protein expression was observed. VDAC1 protein expression was increased after 15 s exposure to He CAP 4 slm. Bottom bar graph shows relative protein levels. (**C**) Rhod-2 AM staining was used to measure changes in intracellular calcium concentration due to erastin treatment. Intracellular calcium concentration was restored after 15 s exposure to He CAP 4 slm. Original magnification, 200 X. Scale bar, 20 μm. The bottom bar graph shows the relative fluorescence levels. (**D**) Schematic diagram of He CAP exposure-induced inflammation and ferroptosis regulation in HGF1 cells. All values are presented as the mean ± SD. Statistical significance was measured using the Mann-Whitney test. *, $P < 0.05$, compared with the control. #, $P < 0.05$, Comparison with cells treated with 10 μM erastin.

fetal bovine serum, 100 U/ml penicillin, and 100 μg/ml streptomycin at 37 °C under a humidified 5% CO2 atmosphere. HGF-1 cells were seeded in 100-mm dishes and cultured to 70 ~ 80% confluence at 37 °C in a CO2 incubator. After 24 h, the medium was replaced with serum free medium, and the cells were pretreated with erastin or N-acetyl cysteine for 1 h, followed by exposure with He CAP. Then, the cells were incubated at 37 °C in a CO2 incubator for 6 h.

Cell viability assay

Cell viability to helium atmospheric pressure plasma time-dependent exposure was analyzed using the LDH-Glo cytotoxicity assay kit (J2380, Promega). HGF-1 cells were seeded in a 24-well cell culture plate and cultured for 24 h. The cells were then exposed to He CAP for 0, 10, 30, 60, 120, and 180 s. Cells were cultured and luminescence was measured using a Microplate Reader Detection System (GloMax® Discover System, Promega).

Helium plasma application

The floating electrode dielectric barrier discharge (FEDBD) plasma device used in this study was designed and fabricated to investigate the anti-inflammatory and regenerative effect of plasma on HGF-1 cells. The electrical properties of the FEDBD plasma device were investigated and measured using an oscilloscope. Plasma discharge was performed at 40 kHz, 6 kV, and 7.5 W using helium (4 L/min, 4 SLM; standard liters per minute) and oxygen (50 SCCM). The distance between the plasma nozzle and the cell was set to 2 cm, and exposure was performed for 10, 30, 60, 120, and 180 s.

	Forward	Reverse
hiNOS	CACCATCCTGGTGGAACTCT	TCCAGGATACCTTGGACCAG
hCOX-2	TACCCTCCTCAAGTCCCTGA	ACTGCTCATCACCCCATTCA
hIL-1β	GGACAAGCTGAGGAAGA TGC	TCGTTATCCCATGTGTCGAA
hTNFα	GGCTCCAGGCGGTGCTTG	GGGCTACAGGCTTGTCAC TCG
hIL-6	AGGAGACTTGCCTGGTG AAA	ACACACCCACCTTTTTCTGC
hGPX4	CTTCCCGTGTAACCAGTTCG	TCACGCAGATCTTGCTGAAC
hNACO4	TAAGCCGTCACCTGGAATGT	GGCTTAAGGGTCAAACTGCC
hVDAC1	GGTGCTCTGGTGCTAGGTTA	CAGCGGTCTCCAACTTCTTG
hGAPDH	GAGTCAACGGATTTGGT CGT	TTGATTTTGGAGGGATCTCG

Table 1. List of primer sequences for qRT-PCR.

mRNA quantification

To quantify mRNA levels, RNA was isolated from HGF-1 cells using TRIzol reagent (Invitrogen). Then, 1 μg of RNA was reverse transcribed to generate cDNA using the AMV Reverse Transcription System (Promega Corp., Madison, WI, USA). Real-time PCR was performed using qPCRBIO SyGreen Blue Mix Separate-ROX (PB20.17-05, PCR Biosystems Inc., Pennsylvania, USA) and CronoSTAR™ 96 Real-Time PCR System (640232, TaKaRa, Japan). The mRNA levels of iNOS, COX-2, IL-1β, TNFα, IL-6, GPX4, NACO4, VDAC1, and GAPDH were quantified and analyzed. The primer sequences used for qRT-PCR are listed in Table 1.

Western blotting analysis

The cells were harvested, washed twice with ice-cold phosphate-buffered saline (PBS), and resuspended in lysis buffer. Cell extracts were obtained by briefly sonicating the cell pellets in RIPA buffer containing 50 mM Tris-HCl (pH 7.2), 5 mM EDTA, 150 mM NaCl, 1% Nonidet P-40, 0.1% SDS, protease inhibitor cocktail (GenDEPOT, P3100-001), and phosphatase inhibitor cocktail (GenDEPOT, P3200-001), followed by centrifugation. The supernatant containing the protein extracts was retained. The proteins were quantified using a Pierce® BCA Protein Assay Kit (Pierce Biotechnology, Inc., Rockford, IL, USA), separated on 8 ~ 12% sodium dodecyl sulfate polyacrylamide gels, and transferred onto nitrocellulose membranes. The blots were blocked at room temperature for 1 h with 5% skim milk in PBS containing 0.1% Tween-20 (PBST). They were successively incubated with the primary antibody (1:2000; overnight at 4 °C), secondary antibody (1:2500), and anti-rabbit horseradish peroxidase-conjugated antibodies. Specific protein bands were visualized using an enhanced chemiluminescence system. ImageJ software was used to quantify band intensity (National Institutes of Health, Bethesda, MD, USA).

Measurement of reactive oxygen species (ROS) generation.

HGF-1 cells were spread on cover glass bottom dishes and pretreated with erastin for 1 h, followed by exposure with He plasma and incubation for 6 h. Intracellular ROS levels were assessed using 5,6-chloromethyl-2',7'-dichlorodihydrofluorescein diacetate (CM-H2DCFDA) (C2827, Invitrogen). The treated HGF-1 cells were incubated with HBSS (without phenol red) containing 10 μM CM-H2DCFH-DA for 20 min at 37 °C. Mitochondrial ROS levels were measured using MitoSOX (HY-D1055, MedChemExpress), which selectively reacts with superoxide. The treated HGF-1 cells were incubated with 5 μM MitoSOX for 30 min at room temperature. Images were acquired using a fluorescence microscope (ECLIPSE Ni, Nikon, Japan) and analyzed using ImageJ software (Ver. 1.53; National Institutes of Health, Bethesda, MD). Images were displayed at 200x magnification.

Mitochondrial membrane potential (MMP) assay

MMP was assessed using a Leica TCS SP8 confocal laser scanning microscope (Leica Microsystems, Mannheim, Germany) with 5,5′,6,6′-tetrachloro-1,1′,3,3′-tetraethylbenzimidazole-carbocyanide iodine (10009172, JC-1 MMP Assay Kit; Cayman Chemical, Ann Arbor, MI, USA). Briefly, HGF-1 cells were treated with 10 μM of erastin and He plasma at 4 slm for 15 s, cultured for 6 h, and stained with JC-1 for 20 min at 37 °C. The live cells were scanned and analyzed using a microscope with a 35-mm confocal special dish. Fluorescence was measured at 488 nm (green) or 530 nm (red) excitation wavelengths and 530 nm (green) or 590 nm (red) emission wavelengths. JC-1 emits red fluorescence when present inside positively charged mitochondria. At lower mitochondrial potential, the internal positive charge decreases and changes to a single ion form, which emits green color. Decrease in the MMP is indicated by a decrease in the red/green fluorescence intensity ratio.

Immunofluorescence

HGF-1 cells (3×10^5) were seeded in a 4-well chamber and cultured at 37 °C for 24 h. The cells were pretreated with 10 μM erastin for 1 h and He plasma for 15 s, followed by incubation under CO_2 for 6 h. The cells were fixed in 4% paraformaldehyde phosphate buffer (Wako) and incubated at 4 °C for 24 h with 100:1 dilution of rabbit monoclonal primary antibodies against GPX4 and VDAC1. After washing, the cells were incubated for 2 h with Cy3 (red fluorescence) goat anti-rabbit antibody (Life Technologies, Carlsbad, CA, USA), which was diluted 1:300 in blocking buffer. Then, phalloidin (Alexa Fluor 488, green fluorescence) was added, and the cells

were incubated for 30 min. After washing, the coverslips were mounted on microslides using the ProLong Gold Antifate Reagent with DAPI (Life Technologies Corporation).

Flow cytometry analysis

After treatment with erastin and He CAP in a serum-free medium, the cells were washed twice with pre-cooled 1X PBS. Then, 100 µl of IC fixation buffer (Intracellular Fixation & Permeabilization Buffer Set, Cat. 88–8824) was added to the cells, followed by incubation for 50 min at room temperature. Next, the cells were washed twice with 2 ml of 1x permeabilization buffer. The conjugated primary antibodies (IL-1β, TNFα, and IL-6-PE-conjugated Ab) were added directly to 100 µl of permeabilization buffer, and the cells incubated for 1 h at room temperature before washing twice with 2 ml of 1X permeabilization buffer. The FACS analysis buffer was added for analysis, and the cells were analyzed using a FACS Caliber flow cytometer (Becton-Dickinson, San Jose, CA, USA).

Lipid peroxidation assay

Cell lipid peroxidation was measured using EZ-lipid peroxidation (TBARS) assay kit (TBA200, Dogen) with MDA as a standard. HGF-1 cells were prepared in 1X PBS containing 1X Butylated Hydroxyanisole (BHT). After homogenization on ice, centrifugation was performed at 13,000 rpm at 4 °C for 5 min, and only the supernatant was transferred to a new tube. The collected supernatant sample was mixed with 200 µl of indicator solution (a solution containing 10 mL of acid reagent and 1 vial of indicator Thiobarbituric Acid) in a microtube. Free MDA was reacted at room temperature for 45 min, and total MDA was reacted at 65 °C for 45 min, then 150 µl each was dispensed into a 96-well microplate, and the absorbance was measured at 540 nm using a plate reader.

Total and reduced glutathione (GSH) measurement

HGF-1 cells (2×10^7) were lysed by pipetting up and down in 500 µl of lysis buffer. The samples were deproteinized using trichloroacetic acid (TCA) and neutralized with sodium bicarbonate (NaHCO3). Total and reduced GSH levels were analyzed using the GSH/GSSG Ratio Detection Assay Kit II (ab205811, Abcam, Cambridge, MA, USA) according to the manufacturer's instructions and a fluorescence-monitoring microplate reader at Ex/Em = 490/520 nm.

Statistical analysis

All data are expressed as mean ± standard deviation (SD). Statistical analysis used the Mann-Whitney test to compare data between two groups. p-values < 0.05 were considered to be statistically significant. All experiments were performed at least thrice.

Data availability

Data availability statementAll data supporting this manuscript are available upon reasonable request of the corresponding authors.

Received: 29 October 2024; Accepted: 10 February 2025
Published online: 03 March 2025

References

1. 1 Kinane, D. F., Stathopoulou, P. G. & Papapanou, P. N. Periodontal diseases. Nat Rev Dis Primers 3, 17038, doi:https://doi.org/10.1038/nrdp.2017.38 (2017).
2. 2 Kononen, E., Gursoy, M. & Gursoy, U. K. Periodontitis: A multifaceted disease of tooth-supporting tissues. J Clin Med 8, doi:https://doi.org/10.3390/jcm8081135 (2019).
3. 3 Graves, D. Cytokines that promote periodontal tissue destruction. J Periodontol 79, 1585–1591, doi:https://doi.org/10.1902/jop.2008.080183 (2008).
4. 4 Usui, M. *et al.* Mechanism of alveolar bone destruction in Periodontitis - Periodontal bacteria and inflammation. Jpn Dent Sci Rev 57, 201–208, doi:https://doi.org/10.1016/j.jdsr.2021.09.005 (2021).
5. 5 Takashiba, S., Naruishi, K. & Murayama, Y. Perspective of cytokine regulation for periodontal treatment: fibroblast biology. J Periodontol 74, 103–110, doi:https://doi.org/10.1902/jop.2003.74.1.103 (2003).
6. 6 Wielento, A., Lagosz-Cwik, K. B., Potempa, J. & Grabiec, A. M. The role of Gingival fibroblasts in the pathogenesis of Periodontitis. J Dent Res 102, 489–496, doi:https://doi.org/10.1177/00220345231151921 (2023).
7. 7 Birkedal-Hansen, H. Role of Matrix metalloproteinases in Human Periodontal diseases. J Periodontol 64 Suppl 5S, 474–484, doi:https://doi.org/10.1902/jop.1993.64.5s.474 (1993).
8. 8 Fadl, A. & Leask, A. Hiding in Plain Sight: Human Gingival Fibroblasts as an Essential, Yet Overlooked, Tool in Regenerative Medicine. *Cells-Basel* 12, doi:ARTN 2021
9. https://doi.org/10.3390/cells12162021 (2023).
10. 9 Van Dyke, T. E. & Sima, C. Understanding resolution of inflammation in periodontal diseases: is chronic inflammatory periodontitis a failure to resolve? Periodontol 2000 82, 205–213, doi:https://doi.org/10.1111/prd.12317 (2020).
11. 10 Delima, A. J., Karatzas, S., Amar, S. & Graves, D. T. Inflammation and tissue loss caused by periodontal pathogens is reduced by interleukin-1 antagonists. J Infect Dis 186, 511–516, doi:https://doi.org/10.1086/341778 (2002).
12. 11 Han, H., Zhang, G., Zhang, X. & Zhao, Q. Nrf2-mediated ferroptosis inhibition: a novel approach for managing inflammatory diseases. Inflammopharmacology 32, 2961–2986, doi:https://doi.org/10.1007/s10787-024-01519-7 (2024).
13. 12 Chen, K. *et al.* Ferroptosis: A New Development Trend in Periodontitis. *Cells* 11, doi:https://doi.org/10.3390/cells11213349 (2022).
14. 13 Zhang, S. *et al.* Role of ferroptosis-related genes in periodontitis based on integrated bioinformatics analysis. PLoS One 17, e0271202, doi:https://doi.org/10.1371/journal.pone.0271202 (2022).
15. 14 Chen, X., Yu, C., Kang, R. & Tang, D. Iron Metabolism in Ferroptosis. Front Cell Dev Biol 8, 590226, doi:https://doi.org/10.3389/fcell.2020.590226 (2020).
16. 15 Rochette, L. *et al.* Lipid peroxidation and Iron metabolism: two Corner stones in the Homeostasis Control of Ferroptosis. Int J Mol Sci 24, doi:https://doi.org/10.3390/ijms24010449 (2022).

17. 16 Li, R. *et al.* Association between periodontal disease and oral squamous cell carcinoma: a systematic review and meta-analysis. Br J Oral Maxillofac Surg 61, 394–402, doi:https://doi.org/10.1016/j.bjoms.2023.05.004 (2023).
18. 17 Javed, F. & Warnakulasuriya, S. Is there a relationship between periodontal disease and oral cancer? A systematic review of currently available evidence. Crit Rev Oncol Hematol 97, 197–205, doi:https://doi.org/10.1016/j.critrevonc.2015.08.018 (2016).
19. 18 Zhang, Y., He, J., He, B., Huang, R. & Li, M. Effect of tobacco on periodontal disease and oral cancer. Tob Induc Dis 17, 40, doi:https://doi.org/10.18332/tid/106187 (2019).
20. 19 Prakash, G. V., Behera, N., Patel, K. & Kumar, A. Concise characterization of cold atmospheric pressure Helium plasma jet. Aip Adv 11, doi:Artn 085329
21. 10.1063/5.0061857 (2021).
22. 20 Dubuc, A. *et al.* Use of cold-atmospheric plasma in oncology: a concise systematic review. Ther Adv Med Oncol 10, 1758835918786475, doi:https://doi.org/10.1177/1758835918786475 (2018).
23. 21 Ghimire, B. *et al.* The role of UV photolysis and molecular transport in the generation of reactive species in a tissue model with a cold atmospheric pressure plasma jet. Appl Phys Lett 114, doi:Artn 093701
24. 10.1063/1.5086522 (2019).
25. 22 Koga-Ito, C. Y. *et al.* Cold Atmospheric plasma as a therapeutic Tool in Medicine and Dentistry. Plasma Chem Plasma P 44, 1393–1429, doi:https://doi.org/10.1007/s11090-023-10380-5 (2024).
26. 23 Barjasteh, A., Kaushik, N., Choi, E. H. & Kaushik, N. K. Cold Atmospheric pressure plasma: a growing paradigm in Diabetic Wound Healing-mechanism and clinical significance. Int J Mol Sci 24, doi:https://doi.org/10.3390/ijms242316657 (2023).
27. 24 He, R. *et al.* The efficacy and safety of cold atmospheric plasma as a novel therapy for diabetic wound in vitro and in vivo. Int Wound J 17, 851–863, doi:https://doi.org/10.1111/iwj.13341 (2020).
28. 25 Nastuta, A. V., Topala, I., Grigoras, C., Pohoata, V. & Popa, G. Stimulation of wound healing by Helium atmospheric pressure plasma treatment. J Phys D Appl Phys 44, doi:Artn 105204
29. https://doi.org/10.1088/0022-3727/44/10/105204 (2011).
30. 26 Shimatani, A. *et al.* In vivo study on the healing of bone defect treated with non-thermal atmospheric pressure gas discharge plasma. PLoS One 16, e0255861, doi:https://doi.org/10.1371/journal.pone.0255861 (2021).
31. 27 Kos, S. *et al.* Safety aspects of atmospheric pressure Helium plasma jet operation on skin: in vivo study on mouse skin. PLoS One 12, e0174966, doi:https://doi.org/10.1371/journal.pone.0174966 (2017).
32. 28 Brun, P. *et al.* Helium generated cold plasma finely regulates activation of human fibroblast-like primary cells. PLoS One 9, e104397, doi:https://doi.org/10.1371/journal.pone.0104397 (2014).
33. 29 Deng, L. *et al.* Molecular mechanisms of ferroptosis and relevance to inflammation. Inflamm Res 72, 281–299, doi:https://doi.org/10.1007/s00011-022-01672-1 (2023).
34. 30 Chen, J., Ou, L., Liu, W. & Gao, F. Exploring the molecular mechanisms of ferroptosis-related genes in periodontitis: a multi-dataset analysis. BMC Oral Health 24, 611, doi:https://doi.org/10.1186/s12903-024-04342-2 (2024).
35. 31 Martínez-García, M. & Hernández-Lemus, E. Periodontal inflammation and systemic diseases: an overview. Front Physiol 12, doi:ARTN 709438
36. https://doi.org/10.3389/fphys.2021.709438 (2021).
37. 32 Scannapieco, F. A. Periodontal inflammation: from gingivitis to systemic disease? Compend Contin Educ Dent 25, 16–25 (2004).
38. 33 Jepsen, S. *et al.* Periodontal manifestations of systemic diseases and developmental and acquired conditions: Consensus report of workgroup 3 of the 2017 World workshop on the classification of Periodontal and Peri-implant diseases and conditions. J Periodontol 89 Suppl 1, S237-S248, doi:https://doi.org/10.1002/JPER.17-0733 (2018).
39. 34 Qiao, S. *et al.* Involvement of ferroptosis in Porphyromonas gingivalis lipopolysaccharide-stimulated periodontitis in vitro and in vivo. Oral Dis 29, 3571–3582, doi:https://doi.org/10.1111/odi.14292 (2023).
40. 35 Zhao, Y., Li, J., Guo, W., Li, H. & Lei, L. Periodontitis-level butyrate-induced ferroptosis in periodontal ligament fibroblasts by activation of ferritinophagy. Cell Death Discov 6, 119, doi:https://doi.org/10.1038/s41420-020-00356-1 (2020).
41. 36 Li, J. *et al.* Ferroptosis: past, present and future. Cell Death Dis 11, 88, doi:https://doi.org/10.1038/s41419-020-2298-2 (2020).
42. 37 Koppula, P., Zhuang, L. & Gan, B. Cystine transporter SLC7A11/xCT in cancer: ferroptosis, nutrient dependency, and cancer therapy. Protein Cell 12, 599–620, doi:https://doi.org/10.1007/s13238-020-00789-5 (2021).
43. 38 Cha, S. & Park, Y. S. Plasma in dentistry. Clin Plasma Med 2, 4–10, doi:https://doi.org/10.1016/j.cpme.2014.04.002 (2014).
44. 39 Yang, Y. *et al.* Inhibition of bacterial growth on zirconia abutment with a Helium cold atmospheric plasma jet treatment. Clin Oral Investig 24, 1465–1477, doi:https://doi.org/10.1007/s00784-019-03179-2 (2020).
45. 40 Stoffels, E., Sakiyama, Y. & Graves, D. B. Cold atmospheric plasma: charged species and their interactions with cells and tissues. Ieee T Plasma Sci 36, 1441–1457, doi:https://doi.org/10.1109/Tps.2008.2001084 (2008).
46. 41 Tian, H. Y. *et al.* The Interplay between Mitochondrial Dysfunction and Ferroptosis during Ischemia-Associated Central Nervous System Diseases. *Brain Sci* 13, doi:ARTN 1367
47. https://doi.org/10.3390/brainsci13101367 (2023).
48. 42 Figueira, T. R. *et al.* Mitochondria as a Source of Reactive Oxygen and Nitrogen Species: from Molecular mechanisms to Human Health. Antioxid Redox Sign 18, 2029–2074, doi:https://doi.org/10.1089/ars.2012.4729 (2013).

Acknowledgements

We appreciate the support of our experimenters.

Author contributions

J. S. Park., Y. I. Jeong. and B. H. Kim. designed the study. J. S. Park. performed the experiments, prepared all figures, and drafted the manuscript. J. S. Park. and Y. I. Jeong. curated and analyzed data. Y. I. Jeong. and B. H. Kim. provided study oversight. All authors reviewed the manuscript and contributed to revisions.

Funding information

This research was supported by a National Research Foundation of Korea (NRF) grant (No. RS-2023-00222390) and the Basic Science Research Project of the National Research Foundation of Korea (NRF) supported by the Korean government (MSIT) (No. 2020R1A2C1003310).

Declarations

Competing interests

The authors declare no competing interests.

Additional information

Supplementary Information The online version contains supplementary material available at https://doi.org/10.1038/s41598-025-89903-3.

Correspondence and requests for materials should be addressed to B.-H.K.

Reprints and permissions information is available at www.nature.com/reprints.

Publisher's note Springer Nature remains neutral with regard to jurisdictional claims in published maps and institutional affiliations.